

Syntheses, structures and immobilization of ruthenium complexes bearing *N,O*-Schiff-base or *N,N'*-diamine ligands functionalized with alkoxysilyl groups

Ai-Quan Jia, Li-Miao Shi, Fule Wu, Zhi-Feng Xin, Qian-Feng Zhang*

Institute of Molecular Engineering and Applied Chemistry, Anhui University of Technology, Ma'anshan, Anhui 243002, PR China



ARTICLE INFO

Article history:

Received 10 November 2017

Received in revised form

6 December 2017

Accepted 11 December 2017

Available online 12 December 2017

Keywords:

Ruthenium(II)

Schiff-base

Heterogeneous catalysis

X-ray structure

Immobilization

ABSTRACT

Condensation of γ -aminopropyltriethoxysilane and substituted salicylaldehydes in ethanol afforded three new Schiff-base compounds $[(EtO)_3Si(CH_2)_3N=CHArOH]$ ($Ar = C_6H_4$, **L1H**; $C_6H_3(4-Cl)$, **L2H**; $C_6H_2(2,4-tBu_2)$, **L3H**). Treatment of $[Ru(NO)Cl_3 \cdot xH_2O]$ with **L1H** in the presence of Et_3N in THF gave a ruthenium nitrosyl complex $[RuCl_2(NO)(\kappa^2-O,N-L1)(OEt_2)]$ (**1**) with a linear $N=N$ moiety. Reactions of $[(\eta^6-p\text{-cymene})RuCl(\mu-Cl)]_2$ with **L1H** or **L2H** in the presence of $AgNO_3$ and Et_3N afforded complexes $[(\eta^6-p\text{-cymene})RuCl(\kappa^2-O,N-L)]$ ($L = L1, 2; L2, 3$). While reaction of $[Ru(CO)_2Cl_2]_n$ and **L3H** in the presence of Et_3N afforded an anionic ruthenium complex $(Et_3NH)[RuCl_2(CO)_2(\kappa^2-O,N-L3)]$ (**4**). Treatment of alkoxysilyl functionalized *N,N'*-diamine compound $N^1-(3-(trimethoxysilyl)propyl)ethane-1,2-diamine$ (**L4**) with $[Ru(PPh_3)_3Cl_2]$ or $[Ru(DMSO)_4Cl_2]$ ($DMSO =$ dimethyl sulfoxide) or $[Ru(COD)Cl_2]_x$ ($COD =$ 1,5-cyclooctadiene) led to formation of complexes $[Ru(PPh_3)_2Cl_2(\kappa^2-N-L4)]$ (**5**), $[Ru(DMSO)_2Cl_2(\kappa^2-N-L4)]$ (**6**), and $[Ru(COD)Cl_2(\kappa^2-N-L4)]$ (**7**), respectively. Complexes **1–7** were characterized by microanalyses, IR and NMR spectroscopies, and their structures were also confirmed by single-crystal X-ray diffraction. Immobilization of complexes **2** and **5** on SBA-15, and characterization of these hybrid heterogeneous catalysts were studied by transmission electron microscopy (TEM), IR and low pressure N_2 adsorption/desorption measurement. The heterogeneous catalysts were also briefly tested for oxidation of benzyl alcohol to benzaldehyde.

© 2017 Published by Elsevier B.V.

1. Introduction

During the last few decades, the coordination and organometallic chemistry of ruthenium complexes has an unprecedented development mainly due to the disclosure of the ever increasing potential of this class of compounds as efficient promoters in versatile catalytic processes [1]. The majority of these ruthenium complexes possess an appropriate balance between the electronic and steric properties within the ligand environment. As a result of their specific structures, these ruthenium complexes exhibit attractive catalytic abilities and particularly an enhanced activity, chemoselectivity and stability in target chemical transformations [2]. Immobilizing ruthenium complexes on solid supports has emerged as a highly effective improvement to enhance their potential as catalysts in chemical reactions [3]. The best way to immobilize ruthenium complexes consists in binding the metal complex through one of its most stable ligands without altering the

catalytic propensity of the initial active site [4]. Being thus equipped, we could optimize the immobilization procedure for ruthenium complexes with bifunctional *N,O*- and *N,N'*-bidentate chelating ligands with alkoxysilyl groups. In general the solid catalyst support should be chemically, thermally and mechanically stable and have a suitably high surface area and an appropriate pore size to allow for the easy diffusion of substrates to and from the active sites [5]. This is an important point, since weak, reversible binding leads to the well-known and feared leaching of catalyst, the detachment of the ruthenium complex and/or the linker from the support [6]. Furthermore, ruthenium complexes with two monodentate linkers are not necessarily bound in a chelating manner, again making them vulnerable to leaching. This problem can be solved by using chelating linkers, which has led us to consider the use of Schiff base as a way to introduce the desired functionality, such as a $-\text{Si}(OR)_3$ group, owing to its ability to condense with surface $-\text{OH}$ groups of inorganic supports and to form sol-gel materials [7]. On the other hand, Schiff bases are common ligands in transition metal chemistry. For example, square-planar Ni(II) complexes of glycine Schiff bases have been widely applied in the

* Corresponding author.

E-mail address: zhangq@ahut.edu.cn (Q.-F. Zhang).

asymmetric synthesis of α -amino acids [8]. In this contribution, we herein report syntheses and structures of ruthenium complexes bearing *N,O*-Schiff base and *N,N'*-diamine ligands functionalized with alkoxyisilyl groups along with immobilization of the typical complexes on SBA-15 and characterization of these hybrid heterogeneous catalysts.

2. Experimental section

2.1. General considerations

All manipulations were carried out under nitrogen by standard Schlenk techniques. Solvents were purified, distilled and degassed prior to use. $[\text{Ru}(\text{PPh}_3)_3\text{Cl}_2]$, $[\text{Ru}(\text{CO})_2\text{Cl}_2]_n$, $[(\eta^6-p\text{-cymene})\text{RuCl}(\mu\text{-Cl})_2]$, $[\text{Ru}(\text{NO})\text{Cl}_3 \cdot x\text{H}_2\text{O}]$, $[\text{Ru}(\text{DMSO})_4\text{Cl}_2]$ (DMSO = dimethyl sulf oxide), and $[\text{Ru}(\text{COD})\text{Cl}_2]_x$ (COD = 1,5-cyclooctadiene) were prepared according to the literature methods [9–14]. Triethylamine, salicylaldehyde, 5-chloro-salicylaldehyde, 3,5-(di-*tert*-butyl)salicylaldehyde, γ -aminopropyltriethoxysilane, and *N*¹-[3-(trimethoxysilyl)-propyl]ethane-1,2-diamine were purchased from Alfa Aesar Ltd. and used as received. NMR spectra were recorded on a Bruker ALX400 spectrometer operating at 400 and 162 MHz for ¹H and ³¹P, respectively. Chemical shifts (δ , ppm) were reported with reference to SiMe₄ (¹H) and 85% H₃PO₄ (³¹P). Infrared spectra were recorded on a Perkin-Elmer 16 PC FT-IR spectrophotometer. Elemental analyses were carried out using a Perkin-Elmer 2400 CHN analyzer. N₂ adsorption/desorption isotherms were obtained at 77 K with a Micromeritics ASAP 2020M+C system after the samples were first degassed at 120 °C for 6 h. TEM images were collected on a JEM-2100 electron microscope at 200 kV. Gas chromatography analyses were performed with an FID detector on a Shimadzu GC-2010 Plus spectrometer using the RTX-5 column.

2.2. Syntheses of ligands

2.2.1. General procedure

Salicylaldehyde (1.80 mmol) and γ -aminopropyl- triethoxysilane (0.41 g, 1.80 mmol) in 20 mL ethanol solution was carried out with stirring at 85 °C for 2 h. Upon cooling to room temperature, the solvent was removed with rotary evaporator. The crude product (yellow oil) was dried in vacuum to afford the desired Schiff-base ligands in excellent yields (ca. > 95%). For L1H: ¹H NMR (CDCl₃, ppm): 8.74 (mbr, 1H, OH), 8.31 (s, 1H, CH=N), 7.29–6.83 (m, 4H, C₆H₄), 3.82–3.75 (m, 6H, O-CH₂), 3.58–3.50 (m, 2H, N-CH₂), 1.81–1.72 (m, 2H, CH₂), 1.22–1.10 (m, 9H, CH₃), 0.67–0.60 (m, 2H, Si-CH₂). IR (KBr disc, cm⁻¹): v_{C-H} = 2914(s), 1457(w), 1369(s), v_{C=N} = 1628(s), v_{C-C} = 1553(m), 791(m), v_{Si-O} = 1082(s), v_{C-O} = 1312(s). For L2H: ¹H NMR (CDCl₃, ppm): 8.79 (mbr, 1H, OH), 8.22 (s, 1H, CH=N), 7.21–6.84 (m, 3H, C₆H₃), 3.80–3.72 (m, 6H, O-CH₂), 3.57–3.51 (m, 2H, N-CH₂), 1.80–1.73 (m, 2H, CH₂), 1.22–1.10 (m, 9H, CH₃), 0.64–0.54 (m, 2H, Si-CH₂). IR (KBr disc, cm⁻¹): v_{C-H} = 2925(s), 1437(w), 1366(s), v_{C=N} = 1618(s), v_{C-C} = 1565(m), 790(m), v_{Si-O} = 1070(s), v_{C-O} = 1296(s). For L3H: ¹H NMR (CDCl₃, ppm): 8.69 (mbr, 1H, OH), 8.32 (s, 1H, CH=N), 7.52–7.48 (m, 2H, C₆H₂), 3.71–3.63 (m, 6H, O-CH₂), 3.45–3.36 (m, 2H, N-CH₂), 1.72 (s, 18H, C-CH₃), 1.35–1.29 (m, 9H, CH₃), 0.65–0.60 (m, 2H, Si-CH₂). IR (KBr disc, cm⁻¹): v_{C-H} = 2935(s), 1445(w), 1371(s), v_{C=N} = 1635(s), v_{C-C} = 1561(m), 778(m), v_{Si-O} = 1070(s), v_{C-O} = 1310(s).

2.3. Syntheses of ruthenium Schiff base complexes functionalized with alkoxyisilyl groups

2.3.1. Synthesis of $[\text{RuCl}_2(\text{NO})(\kappa^2\text{-O},\text{N-L1})(\text{OEt}_2)]$ (1)

Solution of ligand L1H (32.6 mg, 0.10 mmol) in THF (5 mL) was added a solution of $[\text{Ru}(\text{NO})\text{Cl}_3 \cdot x\text{H}_2\text{O}]$ (23.7 mg, 0.10 mmol) in THF (15 mL). To the mixture was added two drops of Et₃N (ca. 0.2 mL).

The solution was then refluxed for 4 h, during which a color changed from light red to dark red. The solvent was removed by vacuum, and the residue was washed with diethyl ether (5 mL × 3) and *n*-hexane (5 mL × 2). Recrystallization from CH₂Cl₂/Et₂O (1:5) gave red block crystals of $[\text{RuCl}_2(\text{NO})(\kappa^2\text{-O},\text{N-L1})(\text{OEt}_2)]$ (1). The solid product was collected and dried in air. Yield: 51 mg, 85%. IR (KBr disc, cm⁻¹): v_{C-H} = 2930(s), 1440(w), 1370(s), v_{N=O} = 1790(s), v_{C=N} = 1625(s), v_{C=C} = 1565(m), 780(m), v_{C-N} = 1455(s), v_{Si-O} = 1075(s), v_{Si-C} = 1268(s). ¹H NMR (CDCl₃, ppm): 8.21 (s, 1H, CH=N), 7.31–6.86 (m, 4H, C₆H₄), 3.82–3.75 (m, 6H, O-CH₂), 3.58–3.50 (m, 2H, N-CH₂), 3.30–3.24 (m, 4H, O-CH₂CH₃), 1.81–1.76 (m, 2H, CH₂), 1.25–1.16 (m, 15H, CH₃), 0.68–0.60 (m, 2H, Si-CH₂). Anal. Calc. for C₂₀H₃₆N₂O₆SiCl₂Ru: C, 40.00; H, 6.04; N, 4.67%. Found: C, 39.12; H, 6.01; N, 4.62%.

2.3.2. Synthesis of $[(\eta^6-p\text{-cymene})\text{RuCl}(\kappa^2\text{-O},\text{N-L1})]$ (2)

To a slurry solution of $[(\eta^6-p\text{-cymene})\text{RuCl}(\mu\text{-Cl})_2]$ (48.9 mg, 0.08 mmol) and AgNO₃ (27.1 mg, 0.16 mmol) in CH₃CN (10 mL) was added a solution of ligand L1H (52.1 mg, 0.16 mmol) and Et₃N (ca. 0.1 mL) in THF (5 mL). The mixture solution was stirred at room temperature for 15 min, resulting in a yellow solution with a white precipitate. The precipitate was removed by filtration. The clear solution was stirred at room temperature for additional 2 h, during which a color changed gradually from yellow to red. The solvent was removed by vacuum, and the residue was washed with diethyl ether (5 mL × 3). Recrystallization from CH₂Cl₂/*n*-hexane (1:3) gave red block crystals of $[(\eta^6-p\text{-cymene})\text{RuCl}(\kappa^2\text{-O},\text{N-L1})]$ (2). The solid product was collected and dried in air. Yield: 87.5 mg, 92%. IR (KBr disc, cm⁻¹): v_{C-H} = 2933(s), 1442(w), 1368(s), v_{C=N} = 1628(s), v_{C-C} = 1569(m), 784(m), v_{C-N} = 1457(s), v_{Si-O} = 1071(s), v_{Si-C} = 1262(s). ¹H NMR (CDCl₃, ppm): 8.11 (s, 1H, CH=N), 7.39–7.07 (m, 8H, -Ar), 3.87–3.80 (m, 6H, O-CH₂), 3.74–3.67 (m, 2H, N-CH₂), 2.92–2.85 (m, 1H, -CH(CH₃)₂), 2.32 (s, 3H, C₆H₄-CH₃), 1.74–1.70 (m, 2H, CH₂), 1.29–1.12 (m, 15H, CH₃), 0.64–0.58 (m, 2H, Si-CH₂). Anal. Calc. for C₂₆H₄₀NO₄SiClRu: C, 52.46; H, 6.77; N, 2.35%. Found: C, 52.38; H, 6.73; N, 2.33%.

2.3.3. Synthesis of $[(\eta^6-p\text{-cymene})\text{RuCl}(\kappa^2\text{-O},\text{N-L2})]$ (3)

The method was similar to that used for 2, employing ligand L2H (65.7 mg, 0.18 mmol) instead of L1H. Yield: 99 mg, 90%. IR (KBr disc, cm⁻¹): v_{C-H} = 2936(s), 1441(w), 1362(s), v_{C=N} = 1624(s), v_{C-C} = 1572(m), 788(m), v_{C-N} = 1462(s), v_{Si-O} = 1074(s), v_{Si-C} = 1261(s). ¹H NMR (CDCl₃, ppm): 8.21 (s, 1H, CH=N), 7.63–6.80 (m, 7H, -Ar), 3.83–3.76 (m, 6H, O-CH₂), 3.72–3.62 (m, 2H, N-CH₂), 2.84–2.78 (m, 1H, -CH(CH₃)₂), 2.23 (s, 3H, C₆H₄-CH₃), 1.83–1.76 (m, 2H, CH₂), 1.28–1.11 (m, 15H, CH₃), 0.68–0.59 (m, 2H, Si-CH₂). Anal. Calc. for C₂₆H₃₉NO₄SiClRu: C, 49.40; H, 6.24; N, 2.22%. Found: C, 49.16; H, 6.33; N, 2.26%.

2.3.4. Synthesis of $(\text{Et}_3\text{NH})[\text{RuCl}_2(\text{CO})_2(\kappa^2\text{-O},\text{N-L3})]$ (4)

To a slurry solution of $[\text{Ru}(\text{CO})_2\text{Cl}_2]_n$ (45.6 mg, 0.2 mmol) in THF (10 mL) was added a solution of ligand L3H (84.0 mg, 0.2 mmol) and Et₃N (ca. 0.1 mL) in THF (5 mL). The mixture solution was stirred at reflux for 4 h, resulting in a yellow solution. The solvent was removed by vacuum, and the residue was washed with diethyl ether (5 mL × 3). Recrystallization from CH₂Cl₂/*n*-hexane (1:4) gave yellow crystals of $(\text{Et}_3\text{NH})[\text{RuCl}_2(\text{CO})_2(\kappa^2\text{-O},\text{N-L3})]$ (4). The solid product was collected and dried in air. Yield: 105 mg, 81%. IR (KBr disc, cm⁻¹): v_{C-H} = 2932(s), 1448(w), 1366(s), v_{C=O} = 2017(vs), 1998(vs), v_{C=N} = 1620(s), v_{C-C} = 1576(m), 782(m), v_{C-N} = 1459(s), v_{Si-O} = 1071(s), v_{Si-C} = 1268(s). ¹H NMR (CDCl₃, ppm): 8.30 (s, 1H, CH=N), 7.51–7.48 (m, 2H, C₆H₂), 3.70–3.60 (m, 6H, O-CH₂), 3.45–3.36 (m, 2H, N-CH₂), 1.72 (s, 18H, C-CH₃), 1.36–1.29 (m, 9H, CH₃), 0.66–0.60 (m, 2H, Si-CH₂). Anal. Calc. for C₃₂H₅₈N₂O₆SiCl₂Ru: C, 50.12; H, 7.62; N, 3.65%. Found: C, 50.24; H, 7.55; N, 3.69%.

2.3.5. Synthesis of $[Ru(PPh_3)_2Cl_2(\kappa^2N\text{-L4})]\cdot CH_2Cl_2$ (**5** \cdot CH_2Cl_2)

$[Ru(PPh_3)_2Cl_2]$ (106.6 mg, 0.11 mmol) and N^1 -(3-(trimethoxysilyl)propyl)ethane-1,2-diamine (**L4**) (25.2 mg, 0.11 mmol) were dissolved in THF (15 mL), and the mixture was refluxed for 4 h during which a color changed from brown to dark red. The solvent was removed by vacuum, and the residue was washed with diethyl ether (5 mL \times 3). Recrystallization from CH_2Cl_2/n -hexane (1:5) gave brownish red crystals of $[Ru(PPh_3)_2Cl_2(\kappa^2N\text{-L4})]\cdot CH_2Cl_2$ (**5** \cdot CH_2Cl_2). The solid product was collected and dried in air. Yield: 87.8 mg, 85%. IR (KBr disc, cm^{-1}): $\nu_{C-H} = 2930(\text{s}), 1440(\text{w}), 1370(\text{s}), \nu_{N-H} = 3445(\text{m}), 1625(\text{s}), 822(\text{m}), \nu_{C=C} = 1565(\text{m}), 780(\text{m}), \nu_{C-N} = 1455(\text{s}), \nu_{Si-O} = 1075(\text{s}), \nu_{Si-C} = 1268(\text{s}). ^1\text{H NMR}$ ($CDCl_3$, ppm): 7.89–7.43 (m, 30H, P-Ph), 3.57 (s, 9H, O- CH_3), 2.95–2.40 (m, 6H, N- CH_2), 2.20–1.86 (m, 3H, NH_2 and NH), 1.57–1.50 (m, 2H, CH_2), 0.58–0.50 (m, 2H, Si- CH_2); $^{31}\text{P NMR}$ ($CDCl_3$, ppm): 28.5, 29.7. Anal. Calc. for $C_{44}H_{52}N_2O_3SiCl_2P_2Ru\cdot(CH_2Cl_2)$: C, 53.84; H, 5.42; N, 2.79%. Found: C, 53.76; H, 5.47; N, 2.83%.

2.3.6. Synthesis of $[Ru(DMSO)_2Cl_2(\kappa^2N\text{-L4})]$ (**6**)

$[Ru(DMSO)_4Cl_2]$ (58.1 mg, 0.12 mmol) and ligand **L4** (28.0 mg, 0.12 mmol) was mixed in THF (15 mL), and the solution was refluxed for 4 h during which a color changed from yellow to red. The solvent was removed by vacuum, and the residue was washed with diethyl ether (5 mL \times 3). Recrystallization from CH_2Cl_2/n -hexane (1:5) gave red crystals of $[Ru(DMSO)_2Cl_2(\kappa^2N\text{-L4})]$ (**6**). The solid product was collected and dried in air. Yield: 33 mg, 48%. IR (KBr disc, cm^{-1}): $\nu_{C-H} = 2933(\text{s}), 1445(\text{w}), 1368(\text{s}), \nu_{N-H} = 3440(\text{m}), 1610(\text{s}), 836(\text{m}), \nu_{C=C} = 1578(\text{m}), 795(\text{m}), \nu_{C-N} = 1453(\text{s}), \nu_{Si-O} = 1068(\text{s}), \nu_{Si-C} = 1270(\text{s}). ^1\text{H NMR}$ ($CDCl_3$, ppm): 3.59 (s, 9H, O- CH_3), 2.91–2.43 (m, 6H, N- CH_2), 2.34 (s, 12H, S- CH_3), 2.21–1.89 (m, 3H, NH_2 and NH), 1.59–1.49 (m, 2H, CH_2), 0.58–0.49 (m, 2H, Si- CH_2). Anal. Calc. for $C_{12}H_{34}N_2O_5SiCl_2S_2Ru$: C, 26.18; H, 6.22; N, 5.09%. Found: C, 26.29; H, 6.31; N, 5.03%.

2.3.7. Synthesis of $[Ru(COD)Cl_2(\kappa^2N\text{-L4})]$ (**7**)

$[Ru(COD)Cl_2]_x$ (62.2 mg, 0.22 mmol) and ligand **L4** (51.2 mg,

0.22 mmol) were mixed in toluene (15 mL), and then the mixture was refluxed for 4 h during which a color changed from red to dark red. The solvent was removed by vacuum, and the residue was washed with diethyl ether (5 mL \times 3). Recrystallization from CH_2Cl_2/n -hexane (1:5) gave red crystals of $[Ru(COD)Cl_2(\kappa^2N\text{-L4})]$ (**7**). The solid product was collected and dried in air. Yield: 77 mg, 68%. IR (KBr disc, cm^{-1}): $\nu_{C-H} = 2928(\text{s}), 1447(\text{w}), 1376(\text{s}), \nu_{N-H} = 3450(\text{m}), 1620(\text{s}), 830(\text{m}), \nu_{C=C} = 1570(\text{m}), 785(\text{m}), \nu_{C-N} = 1458(\text{s}), \nu_{Si-O} = 1078(\text{s}), \nu_{Si-C} = 1278(\text{s}). ^1\text{H NMR}$ ($CDCl_3$, ppm): 4.34–4.08 (m, 4H, $CH=CH$), 3.56 (s, 9H, O- CH_3), 2.95–2.40 (m, 6H, N- CH_2), 2.20–1.85 (m, 11H, NH_2 , NH, and CH_2 in COD), 1.57–1.46 (m, 2H, CH_2), 0.56–0.47 (m, 2H, Si- CH_2). Anal. Calc. for $C_{16}H_{34}N_2O_3SiCl_2Ru$: C, 38.24; H, 6.82; N, 5.57%. Found: C, 38.11; H, 6.75; N, 5.52%.

2.4. X-Ray crystallography

Crystallographic data and experimental details for ruthenium(II) complexes $[RuCl_2(NO)(\kappa^2-O,N\text{-L1})(OEt_2)]$ (**1**), $[(\eta^6-p\text{-cymene})RuCl(\kappa^2-O,N\text{-L1})]$ (**2**), $[(\eta^6-p\text{-cymene})RuCl(\kappa^2-O,N\text{-L2})]$ (**3**), $(Et_3NH)[RuCl_2(CO)_2(\kappa^2-O,N\text{-L3})]$ (**4**), $[Ru(PPh_3)_2Cl_2(\kappa^2N\text{-L4})]\cdot CH_2Cl_2$ (**5** \cdot CH_2Cl_2), $[Ru(DMSO)_2Cl_2(\kappa^2N\text{-L4})]$ (**6**), and $[Ru(COD)Cl_2(\kappa^2N\text{-L4})]$ (**7**) are summarized in Table 1. Intensity data were collected on a Bruker SMART APEX 1000 CCD diffractometer using graphite-monochromated Mo $K\alpha$ radiation ($\lambda = 0.71073 \text{\AA}$). The data were corrected for absorption using the program SADABS [15]. Structures were solved by Direct Methods and refined by full-matrix least-squares on F^2 using the SHELXTL software package [16]. All non-hydrogen atoms were refined anisotropically. The positions of all hydrogen atoms were generated geometrically ($C_{sp^3}-H = 0.96 \text{\AA}$, $C_{sp^2}-H = 0.93 \text{\AA}$ and $N-H = 0.86 \text{\AA}$), assigned isotropic thermal parameters, and allowed to ride on their respective parent carbon atoms before the final cycle of least-squares refinement. In **5** \cdot CH_2Cl_2 , the CH_2Cl_2 solvent was refined with the bond distance restraints due to relatively high thermal factors of two chloride atoms, which may result in the relatively large $R1(wR2)$ values.

Table 1

Crystallographic data and experimental details for $[Ru(L1)(NO)Cl_2(OEt_2)]$ (**1**), $[(\text{cymene})Ru(L1)Cl]$ (**2**), $[(\text{cymene})Ru(L2)Cl]$ (**3**), $(Et_3NH)[Ru(L3)(CO)_2Cl_2]$ (**4**), $[Ru(L4)(PPh_3)_2Cl]\cdot CH_2Cl_2$ (**5** \cdot CH_2Cl_2), $[Ru(L4)(DMSO)_2Cl_2]$ (**6**), and $[(\text{cod})Ru(L4)Cl_2]$ (**7**).

Compound	1	2	3	4	5 \cdot CH_2Cl_2	6	7
empirical formula	$C_{20}H_{36}N_2O_6SiCl_2Ru$	$C_{26}H_{40}NO_4SiClRu$	$C_{26}H_{39}NO_4SiCl_2Ru$	$C_{32}H_{58}N_2O_6SiCl_2Ru$	$C_{45}H_{54}N_2O_3SiCl_4P_2Ru$	$C_{12}H_{34}N_2O_5SiCl_2S_2Ru$	$C_{16}H_{34}N_2O_3SiCl_2Ru$
formula weight	600.57	595.20	629.64	766.86	1003.80	550.59	502.51
crystal system	triclinic	monoclinic	orthorhombic	monoclinic	trigonal	triclinic	triclinic
<i>a</i> (\AA)	10.3115(15)	28.41(3)	12.971(3)	17.3691(11)	44.710(6)	8.7833(13)	9.7857(11)
<i>b</i> (\AA)	12.4954(18)	7.802(8)	8.1325(16)	14.3285(9)		10.9538(16)	10.9909(12)
<i>c</i> (\AA)	12.5051(18)	12.787(12)	28.017(5)	17.9466(11)	12.9277(19)	12.7730(19)	11.1992(13)
$\alpha(^{\circ})$	88.915(2)					103.912(2)	111.707(1)
$\beta(^{\circ})$	67.735(2)	92.552(13)				101.906(2)	96.640(1)
$\gamma(^{\circ})$	71.249(2)					98.734(2)	98.892(1)
<i>V</i> (\AA^3)	1402.2(4)	2831(5)	2955.3(10)	4123.5(4)	22380(6)	1140.6(3)	1085.9(2)
space group	<i>P</i> -1	<i>P</i> 2 ₁ / <i>c</i>	<i>P</i> ca2 ₁	<i>P</i> 2 ₁ / <i>n</i>	<i>R</i> -3	<i>P</i> -1	<i>P</i> -1
<i>Z</i>	2	4	4	4	18	2	2
<i>D</i> _{calc} (g cm^{-3})	1.422	1.396	1.415	1.235	1.341	1.603	1.040
temperature (K)	296(2)	296(2)	296(2)	296(2)	296(2)	296(2)	296(2)
<i>F</i> (000)	620	1240	1304	1616	9324	568	520
$\mu(\text{Mo-K}\alpha)$ (mm^{-1})	0.826	0.721	0.782	0.577	0.657	1.180	1.040
total refln	8753	17317	17379	26961	35778	7048	6820
independent refln	6180	6549	5377	9329	8701	4992	4828
parameters	294	314	322	413	537	233	230
<i>R</i> _{int}	0.0175	0.0504	0.0542	0.0522	0.2244	0.0163	0.0165
<i>R</i> 1 ^a , <i>wR</i> 2 ^b ($I > 2\sigma(I)$)	0.0447, 0.1080	0.0436, 0.0996	0.0413, 0.0876	0.0609, 0.1484	0.0860, 0.2030	0.0381, 0.0937	0.0363, 0.0752
<i>R</i> 1, <i>wR</i> 2 (all data)	0.0683, 0.1240	0.0961, 0.1230	0.0801, 0.1039	0.1474, 0.1920	0.1334, 0.2300	0.0459, 0.0999	0.0499, 0.0829
<i>GOF</i> ^c	1.025	0.995	1.005	0.995	0.906	1.038	1.012
Flack parameter	—	—	0.02(4)	—	—	—	—

^a $R1 = |||F_0| - |F_c|||/|F_0|$.

^b $wR2 = [w(|F_0^2| - |F_c^2|)^2/w|F_0^2|^2]^{1/2}$.

^c $GOF = [w(|F_0| - |F_c|)^2/(N_{\text{obs}} - N_{\text{param}})]^{1/2}$.

2.5. Immobilization of Ru alkoxysilyl complexes **2** and **5** anchored onto SBA-15

1 g SBA-15 was introduced into a three-necked flask connected to a vacuum pump and heated at 473 K for 4 h in order to remove the water and air adsorbed on the surface. 20 mg Complex **2** or **5** were dissolved in toluene which was degassed with N₂ bubbling for 15 min. The activated SBA-15 was suspended into the above solution, and the mixture was stirred at room temperature for 6 h. The excess toluene was removed using a rotary evaporator, and the resulting yellow solid was dried at 80 °C overnight. The product was washed with toluene and diethyl ether until the filtrate became colorless. Finally the brown solid products (**2**)/SBA-15 and (**5**)/SBA-15 were dried in vacuo for 2 h and stored for further applications. IR (KBr) for (**2**)/SBA-15: $\tilde{\nu}$ = 1628 [ν (C=N)] cm⁻¹; for (**5**)/SBA-15: $\tilde{\nu}$ = 1625 [ν (N-H)] cm⁻¹.

2.6. Catalyst testing

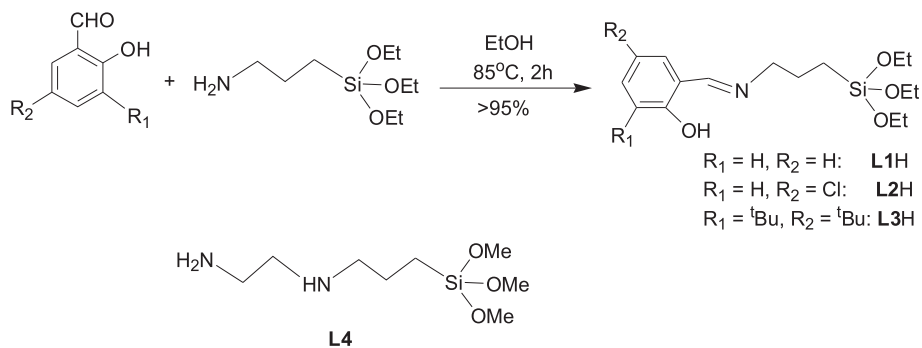
In a typical experiment, a testing tube was filled with benzyl alcohol (1 mmol), TBHP (0.5 mmol), homogeneous catalyst

precursors **2** or **5** or heterogeneous catalyst precursors (**2**)/SBA-15 or (**5**)/SBA-15 (0.02 mmol Ru) and CH₂Cl₂ (10 mL). The resulting suspension was stirred at room temperature for the appropriate times (0.5 h, 1 h, 3 h, 10 h and 20 h). The resulted mixture was filtered, and the filtrate was characterized by gas chromatography using chlorobenzene as internal standard.

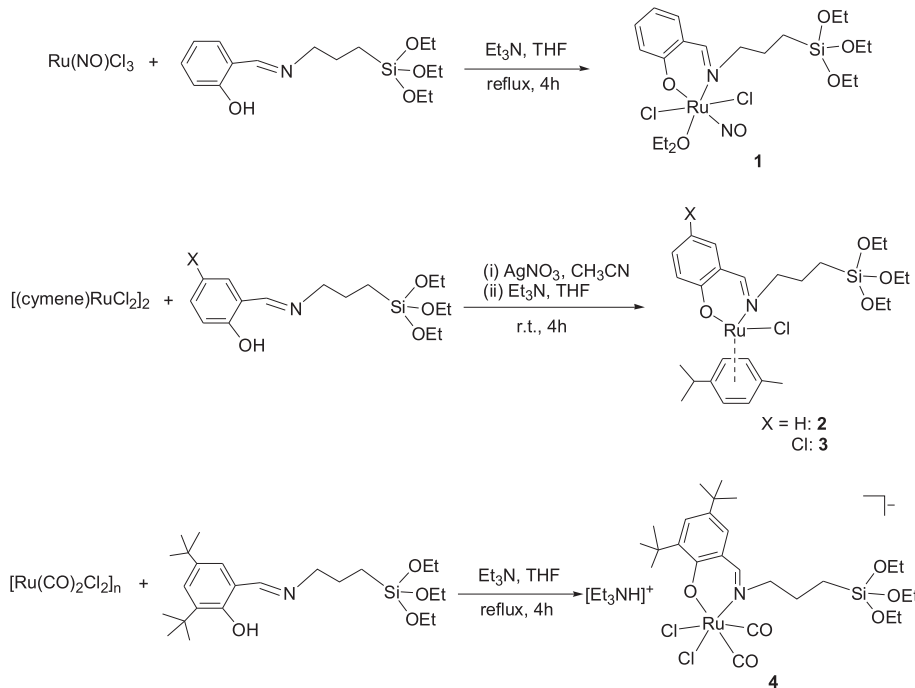
3. Results and discussion

3.1. Preparation and characterization of free ligands and ruthenium complexes

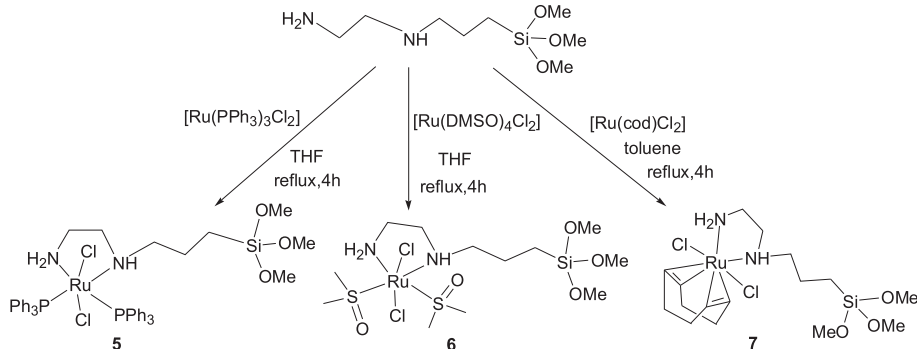
Condensation of γ -aminopropyltriethoxysilane H₂N(CH₂)₃Si(OEt)₃ with salicylaldehyde, 5-chloro-salicylaldehyde, or 3,5-(di-*tert*-butyl)-salicylaldehyde in refluxing ethanol for 2 h easily afforded bidentate Schiff-base ligands **L1H**, **L2H** and **L3H**, respectively (Scheme 1). As shown in Scheme 2, reaction of ruthenium nitrosyl trichloride [Ru(NO)Cl₃ · xH₂O] and **L1H** in the presence of Et₃N in THF resulted a typical ruthenium nitrosyl complex [RuCl₂(NO)(κ^2 -O,N-**L1**)(OEt₂)] (**1**) as red crystals. The deprotonated Schiff-base ligand **L1** and a solvent molecule diethyl ether coordinated to the ruthenium center to



Scheme 1. Syntheses of *N,O*-Schiff bases (**L1H**, **L2H**, **L3H**) and schematic representation of *N,N'*-diamine ligand **L4**.



Scheme 2. Syntheses of ruthenium complexes **1–4** with *N,O*-bidentate Schiff-base ligands bearing ethoxysilyl groups.



Scheme 3. Syntheses of ruthenium complexes 5–7 with *N,N'*-bidentate diamine ligands bearing methoxysilyl groups.

replace one chloro ligand in $[\text{Ru}(\text{NO})\text{Cl}_3 \cdot x\text{H}_2\text{O}]$. The characteristic band for ruthenium nitrosyl complex **1** is found at 1790 cm^{-1} ($\nu_{\text{N}\equiv\text{O}}$) in the IR spectrum, compared with that in a ruthenium nitrosyl species $[\text{Cl}_5\text{Ru}(\text{NO})]^{2-}$ (1843 cm^{-1}) [17], much lower than that of $\text{N}\equiv\text{O}$ group in $[\text{Ru}(\text{NO})(\text{PPh}_3)_2\text{Cl}_3]$ (1881 cm^{-1}) [18]. The Si—O stretching vibration modes were found at 1075 cm^{-1} , similar to that in the free ligand **L1H** (1082 cm^{-1}). Treatment of $[(\eta^6\text{-}p\text{-cymene})\text{RuCl}(\mu\text{-Cl})_2]$ with **L1H** or **L2H** in the presence of two equiv. AgNO_3 and excess Et_3N gave the expected complexes $[(\eta^6\text{-}p\text{-cymene})\text{RuCl}(\kappa^2\text{-O},\text{N}\text{-L1})]$ (**2**) or $[(\eta^6\text{-}p\text{-cymene})\text{RuCl}(\kappa^2\text{-O},\text{N}\text{-L2})]$ (**3**), respectively. The ^1H NMR signals of complexes **2** and **3** showed the methyl protons attached to $-\text{C}_6\text{H}_4$ moiety at around 2.30 ppm as a singlet. Reaction of $[\text{Ru}(\text{CO})_2\text{Cl}_2]_n$ and **L3H** in the presence of Et_3N afforded an anionic ruthenium(II) carbonyl complex $(\text{Et}_3\text{NH})[\text{RuCl}_2(\text{CO})_2(\kappa^2\text{-O},\text{N}\text{-L3})]$ (**4**) as yellow crystals. The two terminal carbonyl $\text{C}\equiv\text{O}$ stretching vibration modes were found at 2017 and 1998 cm^{-1} in the IR spectrum of **4**, and the Si—O stretching vibration modes appeared at 1071 cm^{-1} , which well compared with the related ruthenium carbonyl complex bearing *N,O*-Schiff base ligands functionalized with ethoxysilyl groups [19].

As shown in **Scheme 3**, reactions of *N*'-(3-(trimethoxysilyl)propyl)ethane-1,2-diamine (**L4**) and $[\text{Ru}(\text{PPh}_3)_3\text{Cl}_2]$, $[\text{Ru}(\text{DMSO})\text{Cl}_2]$ or $[\text{Ru}(\text{COD})\text{Cl}_2]_x$ in THF or toluene at reflux afforded the according ruthenium(II) complexes $[\text{Ru}(\text{PPh}_3)_2\text{Cl}_2(\kappa^2\text{N}\text{-L4})]$ (**5**),

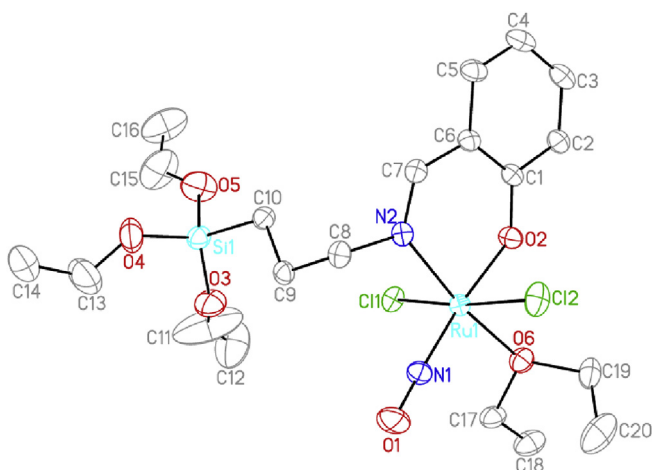


Fig. 1. Molecular structure of complex **1** showing the atom-labeling scheme, hydrogen atoms are omitted for clarity. Thermal ellipsoids are drawn at the 35% probability level. Selected bond lengths (Å) and bond angles (deg): $\text{Ru}(1)\text{-N}(1)=1.719(3)$, $\text{Ru}(1)\text{-N}(2)=2.074(3)$, $\text{Ru}(1)\text{-Cl}(1)=2.3702(10)$, $\text{Ru}(1)\text{-Cl}(2)=2.3722(12)$, $\text{Ru}(1)\text{-O}(2)=1.949(3)$, $\text{Ru}(1)\text{-O}(6)=2.169(3)$, $\text{N}(1)\text{-O}(1)=1.157(4)$, $\text{Si}(1)\text{-C}(10)=1.829(4)$, $\text{Si}(1)\text{-O}(3)=1.581(4)$, $\text{Si}(1)\text{-O}(4)=1.587(4)$, $\text{Si}(1)\text{-O}(5)=1.614(5)$; $\text{O}(2)\text{-Ru}(1)\text{-N}(2)=90.34(11)$, $\text{Cl}(1)\text{-Ru}(1)\text{-Cl}(2)=174.25(4)$, $\text{N}(2)\text{-Ru}(1)\text{-O}(6)=169.29(12)$, $\text{Ru}(1)\text{-N}(1)\text{-O}(1)=177.2(4)$.

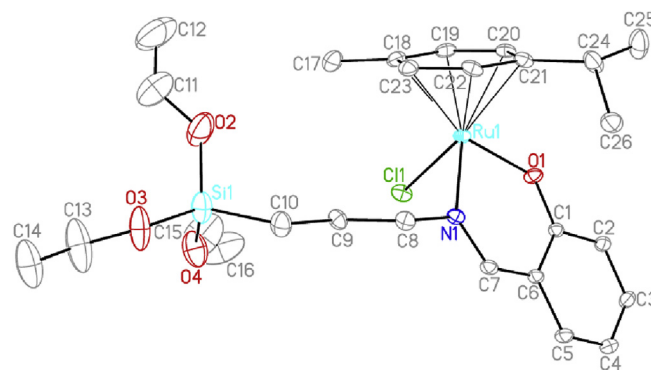


Fig. 2. Molecular structure of complex **2** showing the atom-labeling scheme, hydrogen atoms are omitted for clarity. Thermal ellipsoids are drawn at the 35% probability level. Selected bond lengths (Å) and bond angles (deg): $\text{Ru}(1)\text{-N}(1)=2.091(4)$, $\text{Ru}(1)\text{-Cl}(1)=2.432(2)$, $\text{Ru}(1)\text{-O}(1)=2.041(3)$, $\text{Ru}(1)\text{-C}(18)=2.206(4)$, $\text{Ru}(1)\text{-C}(19)=2.186(4)$, $\text{Ru}(1)\text{-C}(20)=2.177(4)$, $\text{Ru}(1)\text{-C}(21)=2.197(4)$, $\text{Ru}(1)\text{-C}(22)=2.175(4)$, $\text{Ru}(1)\text{-C}(23)=2.183(4)$, $\text{Si}(1)\text{-C}(10)=1.817(6)$, $\text{Si}(1)\text{-O}(2)=1.645(7)$, $\text{Si}(1)\text{-O}(3)=1.629(5)$, $\text{Si}(1)\text{-O}(4)=1.617(6)$; $\text{O}(1)\text{-Ru}(1)\text{-N}(1)=88.25(11)$, $\text{O}(1)\text{-Ru}(1)\text{-Cl}(1)=84.91(10)$.

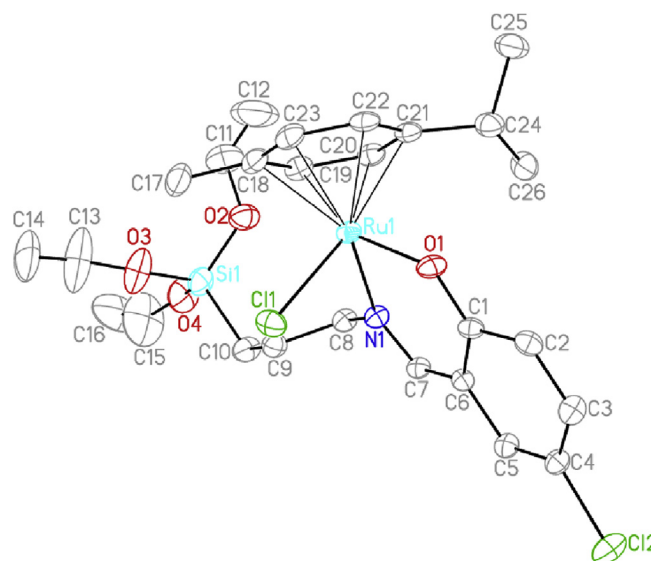


Fig. 3. Molecular structure of complex **3** showing the atom-labeling scheme, hydrogen atoms are omitted for clarity. Thermal ellipsoids are drawn at the 35% probability level. Selected bond lengths (Å) and bond angles (deg): $\text{Ru}(1)\text{-N}(1)=2.095(4)$, $\text{Ru}(1)\text{-Cl}(1)=2.4281(16)$, $\text{Ru}(1)\text{-O}(1)=2.048(4)$, $\text{Ru}(1)\text{-C}(18)=2.229(7)$, $\text{Ru}(1)\text{-C}(19)=2.179(7)$, $\text{Ru}(1)\text{-C}(20)=2.163(5)$, $\text{Ru}(1)\text{-C}(21)=2.183(6)$, $\text{Ru}(1)\text{-C}(22)=2.185(6)$, $\text{Ru}(1)\text{-C}(23)=2.187(6)$, $\text{Si}(1)\text{-C}(10)=1.820(7)$, $\text{Si}(1)\text{-O}(2)=1.625(6)$, $\text{Si}(1)\text{-O}(3)=1.610(7)$, $\text{Si}(1)\text{-O}(4)=1.609(6)$; $\text{O}(1)\text{-Ru}(1)\text{-N}(1)=87.84(19)$, $\text{O}(1)\text{-Ru}(1)\text{-Cl}(1)=84.63(12)$.

[Ru(DMSO)₂Cl₂(κ^2 N-**L4**)] (**6**) or [Ru(COD)Cl₂(κ^2 N-**L4**)] (**7**), respectively, as red crystals in good yields. The ³¹P NMR spectrum of **5** displayed phosphorus resonances at 28.5 and 29.7 ppm, indicating the two triphenylphosphine ligands are *cis* to each other. The chemical shifts of methyl groups in DMSO ligands in **6** were found at around 2.34 ppm, and the CH=CH protons of COD ligand in **7** were observed in the 4.34–4.08 ppm regions. Moreover, the -NH/NH₂ groups in complexes **5–7** were observed in the 1.85–2.21 ppm

regions in the ¹H NMR spectra. The highfield chemical shift (~0.58 ppm) of -CH₂Si(OMe)₃ protons in complexes **5–7** are near to those of -CH₂Si(OEt)₃ protons in **1–4** (~0.68 ppm). The Si–O stretching vibration modes appeared at around 1070 cm⁻¹ in the IR spectra of complexes **5–7**, similar to those in complexes **1–4**.

3.2. X-ray crystal structures of ruthenium complexes **1–7**

It was noted that crude products of complexes **1–7** were all initially obtained as oily states, which could not be purified by chromatograph over silica gel, due to the attachment of alkoxyisilyl groups on the expected targets. Many efforts have been performed so as to obtain pure products of complexes **1–7** by repeatable recrystallization under different conditions. Notwithstanding, relatively high/good quality single-crystals of complexes **1–7** were successfully obtained, although it was a quite hard work during our experiments. The ORTEP representations of the molecular structures of them with selected bond distances and bond angles are shown in Figs. 1–7, respectively. The central ruthenium atom in complex **1** is bonded in a slightly distorted octahedral geometry, to two terminal chlorides, two nitrogen atoms (one linear nitrosyl ligand and the other one is imine nitrogen) and two oxygen atoms (one phenolic oxygen and one diethyl ether molecule). The Ru–N_{NO} bond length is 1.719(3) Å and the N≡O bond length is 1.157(4) Å, which are compared with those in other ruthenium(II) nitrosyl complexes [18,20], e.g. [RuCl₃(NO)(PPh₃)₂] (1.737(7) Å for Ru–N, 1.142(8) Å for N≡O). In addition, the Ru–N–O bond angle is 177.2(4)°, clearly indicating a linear N≡O coordination where Ru^{II}–NO⁺ is the electronic structure. The Ru–O_{Et₂O} bond length of 2.169(3) Å is longer than that of Ru–O(**L1**) (1.949(3) Å), presenting a relatively weaker interaction. The Ru–N(**L1**) bond length of 1.949(3) Å and the average Ru–Cl bond length of 2.3712(11) Å are in agreement with the corresponding bond parameters as described for similarly constituted complexes [19,21]. The Si–C and average Si–O bond lengths are 1.829(4) and 1.594(4) Å, respectively. The bite angle of O–Ru–N is 90.34(11)° in complex **1**. Complexes **2** and **3** could be formulated as a six-coordinate ruthenium species assuming the cymene moiety occupied three coordination sites, the bite angles of O–Ru–N are 88.25(11)° and 87.84(19)° in complexes **2** and **3**, respectively, smaller than that in complex **1** (90.34(11)°). In the anionic ruthenium complex **4**, the ruthenium atom is

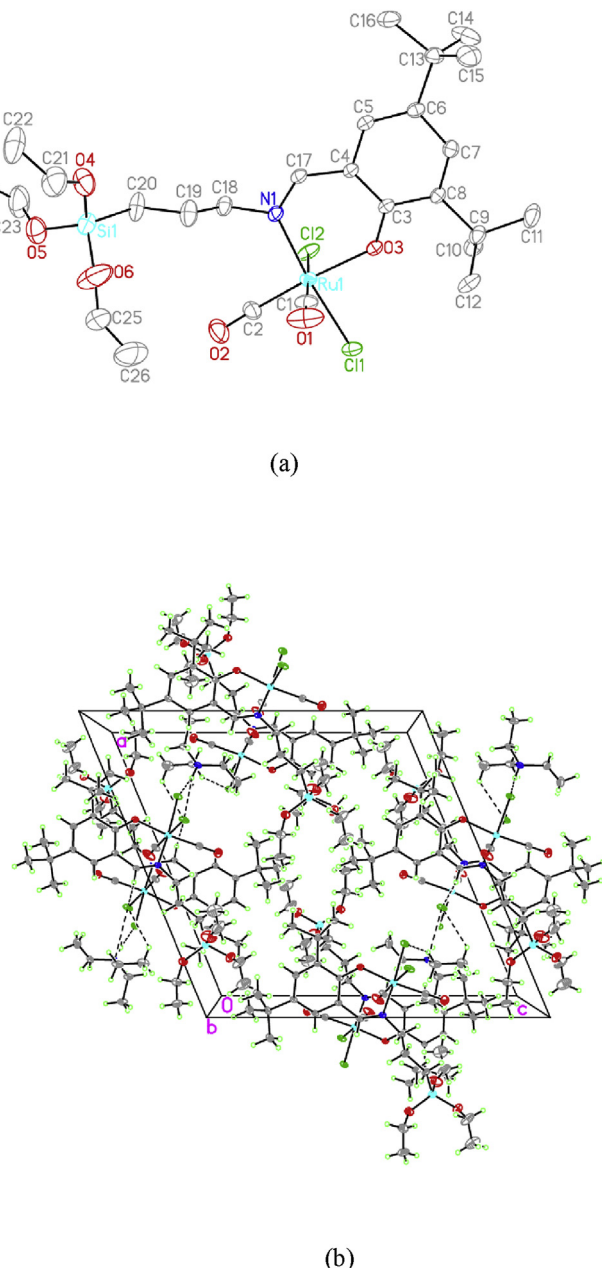


Fig. 4. (a) Molecular structure of complex **4** showing the atom-labeling scheme, hydrogen atoms and the counter cation are omitted for clarity. Thermal ellipsoids are drawn at the 35% probability level. Selected bond lengths (Å) and bond angles (deg): Ru(1)-C(1) = 1.838(9), Ru(1)-C(2) = 1.848(9), Ru(1)-Cl(1) = 2.4120(14), Ru(1)-Cl(2) = 2.4291(16), Ru(1)-N(1) = 2.065(4), Ru(1)-O(3) = 2.031(4), O(1)-C(1) = 1.071(8), O(2)-C(2) = 1.128(8), Si(1)-C(20) = 1.791(7), Si(1)-O(4) = 1.581(6), Si(1)-O(5) = 1.560(6), Si(1)-O(6) = 1.576(9); N(1)-Ru(1)-O(3) = 89.17(15), N(1)-Ru(1)-Cl(1) = 173.26(13), C(1)-Ru(1)-Cl(2) = 178.4(3), C(2)-Ru(1)-O(3) = 173.9(2), O(1)-C(1)-Ru(1) = 178.3(7), O(2)-C(2)-Ru(1) = 176.1(9). (b) Packing diagram of anionic ruthenium complex **4** in a unit cell, viewed along the crystallographic ac plane. C–H···Cl, N–H···Cl, and C–H_{CH=N}···Cl intermolecular hydrogen bonds are shown as dashed lines.

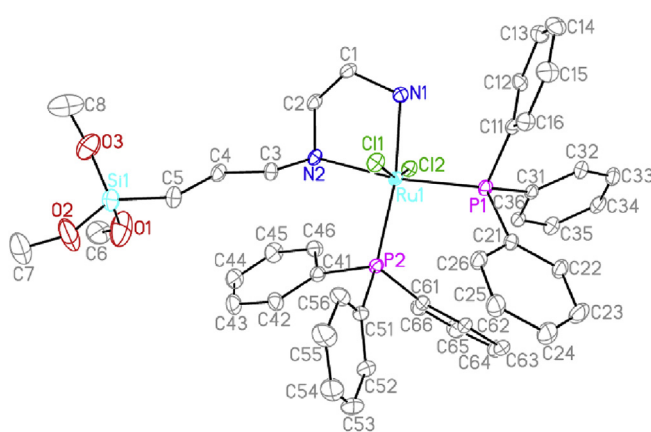
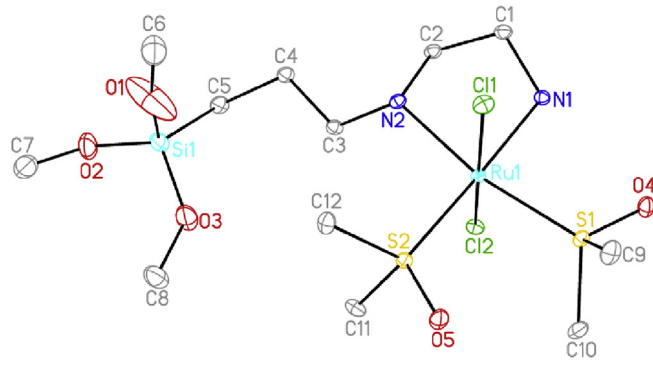
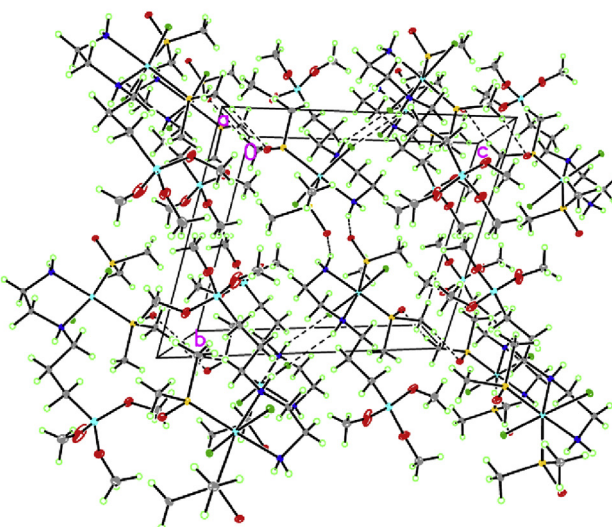


Fig. 5. Molecular structure of complex **5** showing the atom-labeling scheme, hydrogen atoms and the solvent are omitted for clarity. Thermal ellipsoids are drawn at the 35% probability level. Selected bond lengths (Å) and bond angles(deg): Ru(1)-N(1) = 2.149(5), Ru(1)-N(2) = 2.214(5), Ru(1)-Cl(1) = 2.4250(18), Ru(1)-Cl(2) = 2.4184(18), Ru(1)-P(1) = 2.3272(17), Ru(1)-P(2) = 2.333(2), Si(1)-C(5) = 1.824(7), Si(1)-O(1) = 1.614(9), Si(1)-O(2) = 1.604(9), Si(1)-O(3) = 1.549(9); N(1)-Ru(1)-N(2) = 78.9(2), P(1)-Ru(1)-P(2) = 97.77(6), Cl(1)-Ru(1)-Cl(2) = 164.08(7), N(2)-Ru(1)-P(1) = 171.19(15), N(1)-Ru(1)-P(2) = 169.55(14).

coordinated by two carbonyl groups, two chloro ligands and one κ^2 -*O,N* Schiff-base ligand. The Ru–C bond lengths are 1.838(9) and 1.848(9) Å, which are compared with those in the already-known ruthenium(II) carbonyl complexes [22]. The O–Ru–N bite angle of the bidentate Schiff-base ligand is 89.17(15)°, being slightly larger than those in other ruthenium(II) carbonyl complexes with Schiff-base ligands (87.49(10)°–88.19(10)°) [20]. The crystal packing molecule of complex **4** is governed by the weak intermolecular N–H···Cl and C–H···Cl hydrogen-bonding interactions between the anionic ruthenium moiety and the counter cation [Et₃NH]⁺, moreover there is also hydrogen-bonding interactions of C–H_{CH=N}···Cl between two ruthenium molecules as shown in Fig. 4(b).



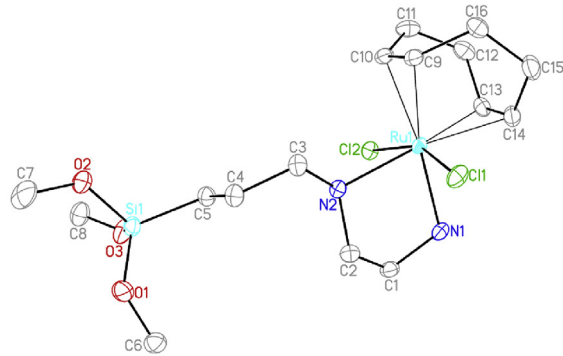
(a)



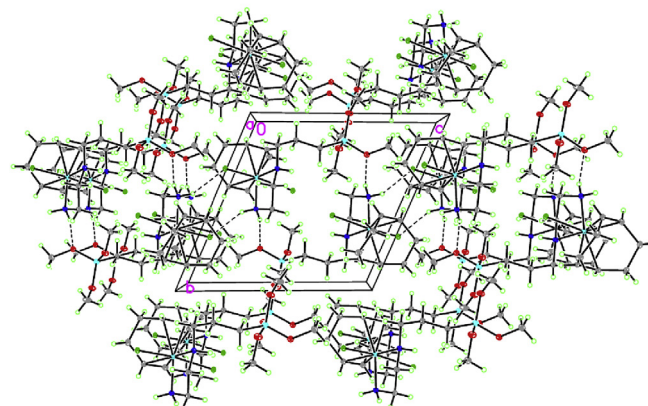
(b)

Fig. 6. (a) Molecular structure of complex **6** showing the atom-labeling scheme, hydrogen atoms are omitted for clarity. Thermal ellipsoids are drawn at the 35% probability level. Selected bond lengths (Å) and bond angles(deg): Ru(1)–N(1) = 2.128(3), Ru(1)–N(2) = 2.187(3), Ru(1)–Cl(1) = 2.4089(9), Ru(1)–Cl(2) = 2.4056(9), Ru(1)–S(1) = 2.2462(10), Ru(1)–S(2) = 2.2528(9), S(1)–O(4) = 1.488(3), S(2)–O(5) = 1.489(3), Si(1)–C(5) = 1.848(5), Si(1)–O(1) = 1.534(6), Si(1)–O(2) = 1.612(5), Si(1)–O(3) = 1.586(5); N(1)–Ru(1)–N(2) = 79.43(11), S(1)–Ru(1)–S(2) = 92.68(3), Cl(1)–Ru(1)–Cl(2) = 174.40(3), N(2)–Ru(1)–S(1) = 168.32(8), N(1)–Ru(1)–S(2) = 178.13(8). (b) Packing diagram of ruthenium complex **6** in a unit cell, viewed along the crystallographic bc plane. N–H···O_{DMSO} and N–H···Cl intermolecular hydrogen bonds are shown as dashed lines.

The structures of ruthenium complexes **5**–**7** with κ^2 -*N*–**L4** ligand have similar geometry, the two chloro ligands are *trans* to each other with the bond angles of Cl–Ru–Cl being 164.08(7)° in complex **5**, 174.40(3)° in complex **6**, and 159.07(3)° in complex **7**. The bite angles of N–Ru–N are 78.9(2)° in complex **5**, 79.43(11)° in complex **6**, and 80.80(10)° in complex **7**, indicating the different neutral ligands of triphenylphosphine, DMSO and COD coordinated to ruthenium centers have little effect on the bite angle of diamine ligand **L4**. The Ru–N bond lengths are 2.149(5) and 2.214(5) Å in complex **5**, which are similar to those in complex **6** (2.128(3), 2.187(3) Å) and complex **7** (2.123(2), 2.173(3) Å). The average Ru–Cl bond length is 2.4217(18) Å in complex **5**, compared well to those in complex **6** (2.4072(9) Å) and complex **7** (2.4349(8) Å). Moreover, the average Ru–P bond length of 2.330(2) Å in complex **5**, Ru–S bond length of 2.2495(9) Å in complex **6**, and Ru–C bond length of 2.213(3) Å in complex **7** are in good agreement with related



(a)

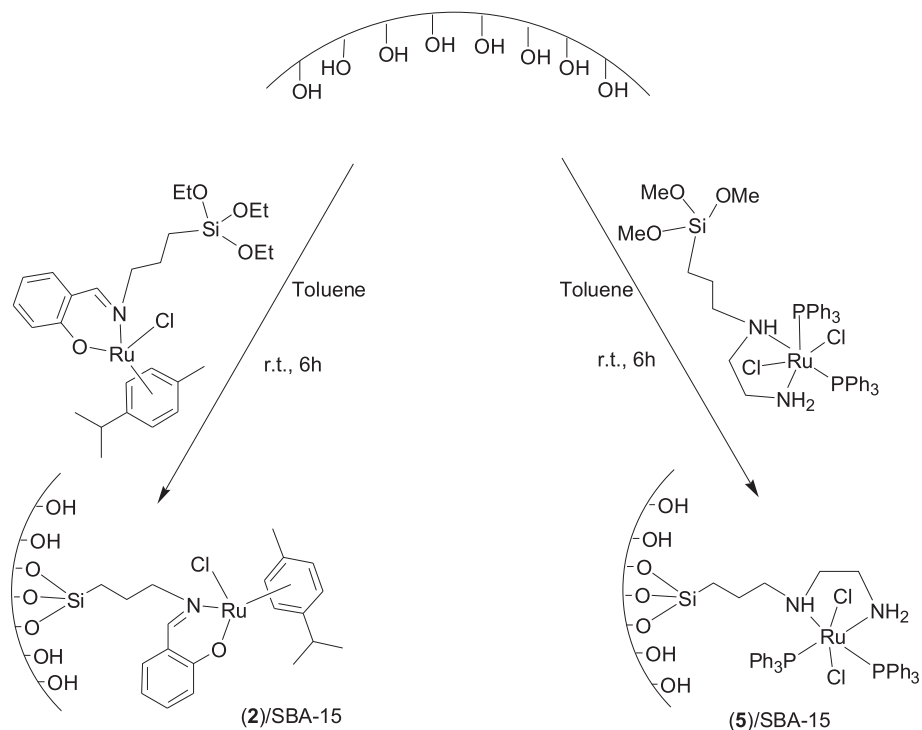


(b)

Fig. 7. (a) Molecular structure of complex **7** showing the atom-labeling scheme, hydrogen atoms are omitted for clarity. Thermal ellipsoids are drawn at the 35% probability level. Selected bond lengths (Å) and bond angles(deg): Ru(1)–N(1) = 2.123(2), Ru(1)–N(2) = 2.173(3), Ru(1)–Cl(1) = 2.4253(8), Ru(1)–Cl(2) = 2.4445(8), Ru(1)–C(9) = 2.225(3), Ru(1)–C(10) = 2.218(3), Ru(1)–C(13) = 2.204(3), Ru(1)–C(14) = 2.206(3), Si(1)–C(5) = 1.839(3), Si(1)–O(1) = 1.617(3), Si(1)–O(2) = 1.618(3), Si(1)–O(3) = 1.629(3); N(1)–Ru(1)–N(2) = 80.80(10), Cl(1)–Ru(1)–Cl(2) = 159.07(3). (b) Packing diagram of ruthenium complex **7** in a unit cell, viewed along the crystallographic bc plane. N–H···O and N–H···Cl intermolecular hydrogen bonds are shown as dashed lines.

ruthenium(II) $\text{PPh}_3/\text{DMSO}/\text{COD}$ complexes comprising N,N' -diamine ligands [23]. Two kinds of hydrogen-bonding interactions of $\text{N}-\text{H}\cdots\text{Cl}$ and $\text{N}-\text{H}\cdots\text{O}_{\text{DMSO}}$ exist in the crystal packing molecule of complex **6** as could be seen in Fig. 6(b). The crystal packing

molecule of complex **7** is governed by the weak intermolecular $\text{N}-\text{H}\cdots\text{Cl}$ and $\text{N}-\text{H}\cdots\text{O}_{\text{Si}(\text{OMe})}$ hydrogen-bonding interactions between the ruthenium molecules to form a one dimensional chain as shown in Fig. 7(b).



Scheme 4. Immobilization of ruthenium complexes **2** and **5** with N,O - or N,N' -bidentate ligand bearing alkoxysilyl group on SBA-15 by condensation.

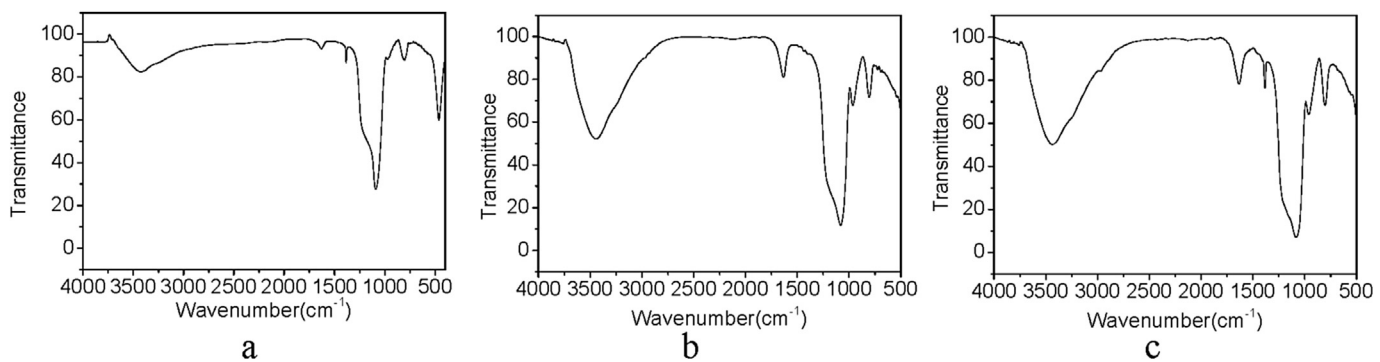


Fig. 8. Infrared spectra of SBA-15 (a), (2)/SBA-15 (b) and (5)/SBA-15 (c).

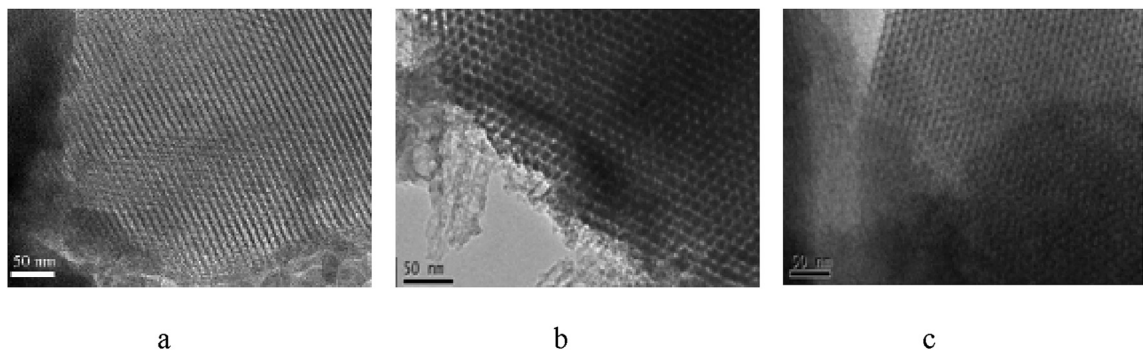


Fig. 9. TEM images of SBA-15 (2)/SBA-15 (b) and (5)/SBA-15 (c).

3.3. Preparation, characterization and application of SBA-15 supported ruthenium complexes

Immobilization of two typical ruthenium complexes **2** and **5** bearing *N,O*-Schiff base or *N,N'*-diamine ligand functionalized with alkoxy silane groups on mesoporous SBA-15 by condensation is shown in Scheme 4, in the loading process, the organic silicon group was connected with SBA-15 in the form of -Si-O-Si-, and one of the silicon-group connected with the organometallic ruthenium complex [24]. The supported ruthenium complexes were further characterized by a series of methods such as IR, TEM and N₂ adsorption/desorption measurements. IR spectra of parent calcined mesoporous SBA-15 and grafted samples show bands at 1206 and 794 cm⁻¹, which are due to stretching vibrations of the mesoporous framework (Si—O—Si) [25], as could be seen in Fig. 8. The imine and amine stretching vibrations around 1628 cm⁻¹ can be observed in the grafted materials, evidencing the presence of the ruthenium complexes in the channels of both mesoporous materials. Moreover, the well supported organic silicon ruthenium complexes were also tested by TEM. The supported materials displayed the similar ordered mesoporous structure compared with SBA-15 (Fig. 9). The particles of the ruthenium complexes loaded on the channel cannot be seen in the TEM images, however, the channel of unsupported SBA-15 seemed clearly visible while the channel of (**2**)/SBA-15 and (**5**)/SBA-15 was obviously unclear, which may be attributed the loading of complexes **1** and **5** on the pore wall of SBA-15 [26].

The pore structures of SBA-15, (**2**)/SBA-15 and (**5**)/SBA-15 were further detected by low pressure N₂ adsorption/desorption measurement at 77 K, as displayed in Fig. 10. The characteristic shape of the N₂ sorption isotherms (type IV isotherm with an H1 hysteresis loop) of (**2**)/SBA-15 and (**5**)/SBA-15 did not change. And the obvious decrease of N₂ uptakes and surface area indicated part of the original pore structure of SBA-15 was occupied by the organic silicon ruthenium complexes [27]. The pore width distributions of (**2**)/SBA-15 (5.92 nm) and (**5**)/SBA-15 (5.98 nm) were smaller than that of the bare SBA-15 (6.24 nm), an indicative of the ruthenium complex occupied partial pore volume. Moreover, the BET surface area are decreased from 695 m² g⁻¹ (SBA-15) to 541 m² g⁻¹ ((**2**)/SBA-15) or 550 m² g⁻¹ ((**5**)/SBA-15). The above results were caused by the loading of complexes **2** and **5** on the pore of SBA-15, which is in accordance with the results of the TEM images.

Previously, Leung reported that alkylruthenium complexes with -CH₂SiMe₃ groups anchored on SBA-15 by elimination of SiMe₄ and the Ru-grafted species could catalyze the oxidation of benzyl alcohol with *tert*-butyl hydroperoxide (TBHP) in moderate yields (up to 70%) [28]. Under this guidance, we took the study of heterogeneous materials (**2**)/SBA-15 and ((**5**))/SBA-15 for oxidation of benzyl alcohol with TBHP as oxidant at room temperature. Treatment of benzyl alcohol with (**2**)/SBA-15 and TBHP in CH₂Cl₂ gave benzaldehyde selectively in 65% yield in 10 h; no benzoic acid was detected. Longer reaction time did not lead to improved yield. Similar yield of benzaldehyde were found with ((**5**))/SBA-15 as catalyst after 10 h of reaction (62%), compared with the homogeneous tetradentate-Schiff-base-ruthenium/NMO (NMO = *N*-methylmorpholine-*N*-oxide) catalytic system (yield up to 77%) [29]. However, the homogeneous catalysts **2** and **5** here were less active than the corresponding supported catalysts, giving yields of 22% and 26%. The immobilized complex (**2**)/SBA-15 appeared to be reusable for four cycles for the oxidation of benzyl alcohol; though longer reaction periods are needed for reactions after the third cycle.

In summary, three new bidentate Schiff-base compounds functionalized with terminal triethoxysilyl groups were synthesized. They were applied to the neutral and anionic ruthenium(II) complexes **1–4**. Reactions of *N*¹-[3-(trimethoxysilyl)-propyl]ethane-1,2-diamine and different ruthenium starting materials

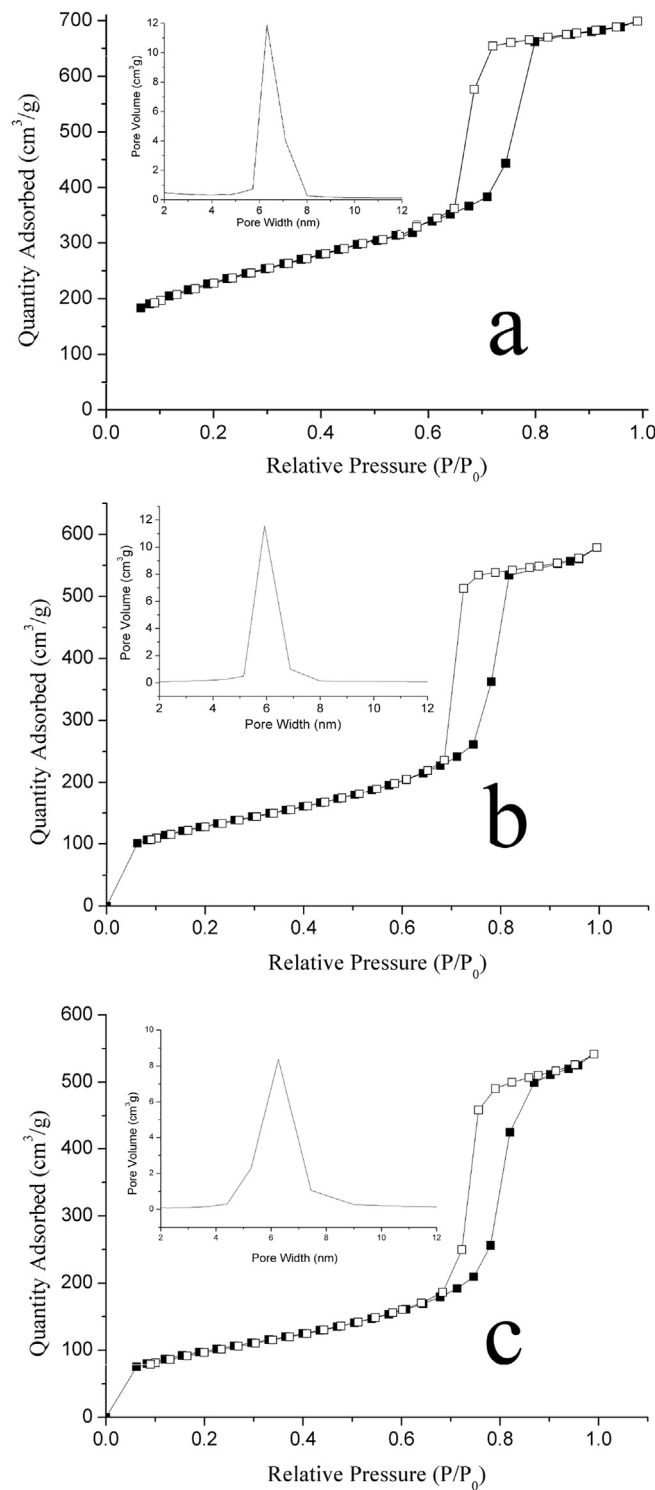


Fig. 10. N₂ sorption isotherms of SBA-15 (a), (**2**)/SBA-15 (b), and (**5**)/SBA-15 (c). The insets were the corresponding pore size distribution curves.

afforded corresponding ruthenium(II) complexes **5–7** bearing κ^2N -diamine ligand with trimethoxysilyl groups. The structures of complexes **1–7** were unambiguously established by single-crystal X-ray diffraction. Up to now, there are few reported ruthenium complexes bearing organosilicone moieties according to CCDC searching result [19,30]. Immobilization of two typical ruthenium(II) complexes **2** and **5** on SBA-15, and characterization of

these hybrid heterogeneous materials were studied by IR, TEM and N₂ adsorption/desorption measurements. The grafted materials were employed as heterogeneous catalysts for oxidation of benzyl alcohol to benzaldehyde and could be recycled several times. Application of such organometallic chemistry of the surface-bound Ru alkoxysilyl species for other organic transformation reactions is underway in our laboratory.

Supplementary material

Crystallographic data for [RuCl₂(NO)(κ²-O,N-L1)(OEt₂)] (**1**), [(η⁶-p-cymene)RuCl(κ²-O,N-L1)] (**2**), [(η⁶-p-cymene)RuCl(κ²-O,N-L2)] (**3**), (Et₃NH)[RuCl₂(CO)₂(κ²-O,N-L3)] (**4**), [Ru(PPh₃)₂Cl₂(κ²N-L4)]·CH₂Cl₂ (**5**·CH₂Cl₂), [Ru(DMSO)₂Cl₂(κ²N-L4)] (**6**), and [Ru(COD)Cl₂(κ²N-L4)] (**7**) have been deposited with the Cambridge Crystallographic Data Center as supplementary publication nos. CCDC 1577451–1577457, respectively. Copies of the data can be obtained free of charge on application to CCDC, 12 Union Road, Cambridge CB2 1EZ, UK [fax: (+44)1233-336-033; e-mail: deposit@ccdc.cam.ac.uk].

Acknowledgements

This project was supported by the Natural Science Foundations of China (21372007 and 21471003).

References

- [1] (a) Q. Zeng, F.W. Lewis, L.M. Harwood, F. Hartl, Role of ligands in catalytic water oxidation by mononuclear ruthenium complexes, *Coord. Chem. Rev.* 304 (2015) 88–101;
 (b) C. Gunathan, D. Milstein, Bond activation and catalysis by ruthenium pincer complexes, *Chem. Rev.* 114 (2014) 12024–12087;
 (c) L. Ackermann, Carboxylate-assisted ruthenium-catalyzed alkyne annulations by C-H/Het-H bond functionalizations, *Accounts Chem. Res.* 47 (2014) 281–295;
 (d) M.B. Herbert, R.H. Grubbs, Z-selective cross metathesis with ruthenium catalysts: synthetic applications and mechanistic implications, *Angew. Chem. Int. Ed.* 54 (2015) 5018–5024.
- [2] (a) M. Zhang, H. Neumann, M. Beller, Selective ruthenium-catalyzed three-component synthesis of pyrroles, *Angew. Chem. Int. Ed.* 52 (2013) 597–601;
 (b) L.M. Geary, J.C. Leung, M.J. Krische, Ruthenium-catalyzed reductive coupling of 1,3-enynes and aldehydes by transfer hydrogenation: anti-diastereoselective carbonyl propargylation, *Chem. Eur. J.* 18 (2012) 16823–16827;
 (c) T.S. Ahmed, R.H. Grubbs, Fast-initiating, ruthenium-based catalysts for improved activity in high E-selective cross metathesis, *J. Am. Chem. Soc.* 139 (2017) 1532–1537;
 (d) B.L. Quigley, R.H. Grubbs, Ruthenium-catalysed Z-selective cross metathesis of allylic-substituted olefins, *Chem. Sci.* 5 (2014) 501–506.
- [3] (a) D.J. Mihalcik, W. Lin, Mesoporous silica nanosphere supported ruthenium catalysts for asymmetric hydrogenation, *Angew. Chem. Int. Ed.* 47 (2008) 6229–6232;
 (b) C.S. Gill, K. Venkatasubbaiah, C.W. Jones, Recyclable polymer- and silica-supported ruthenium(II)-salen bis-pyridine catalysts for the asymmetric cyclopropanation of olefins, *Adv. Synth. Catal.* 351 (2009) 1344–1354;
 (c) S. Syukri, W. Sun, F.E. Kühn, Immobilization of ruthenium(II) salen complexes on poly(4-vinylpyridine) and their application in the catalytic aldehyde olefination, *Tetrahedron Lett.* 48 (2007) 1613–1617.
- [4] C. Bianchini, V.D. Santo, A. Meli, W. Oberhauser, R. Psaro, F. Vizza, Preparation, characterization, and performance of the supported hydrogen-bonded ruthenium catalyst [(sulphos)Ru(NCMe)₃](OSO₂CF₃)/SiO₂. Comparisons with analogous homogeneous and aqueous-biphase catalytic systems in the hydrogenation of benzylideneacetone and benzonitrile, *Organometallics* 19 (2000) 2433–2444.
- [5] N. Linares, A.E. Sepúlveda, M.C. Pacheco, J.R. Berenguer, E. Lalinde, C. Nájera, J. García-Martínez, Synthesis of mesoporous metal complex-silica materials and their use as solvent-free catalysts, *New J. Chem.* 35 (2011) 225–234.
- [6] T. Posset, F. Rominger, J. Blümel, Immobilization of bisphosphinoamine linkers on silica: identification of previous unrecognized byproducts via ³¹P CP/MAS and suspension HR-MAS studies, *Chem. Mater.* 17 (2005) 586–595.
- [7] (a) T. Posset, J. Guenther, J. Pope, T. Oeser, J. Blümel, Immobilization Sonogashira catalyst systems: new insights by multinuclear HRMAS NMR studies, *Chem. Commun.* 47 (2011) 2059–2061;
 (b) N.C. Mehendale, M. Lutz, A.L. Spek, R.J.M.K. Gebbink, G. van Koten, Self-assembly of para-OH functionalized ECE-metallated pincer complexes, *J. Organomet. Chem.* 693 (2008) 2971–2981.
- [8] (a) A.E. Sorochinsky, J.L. Aceña, H. Moriwaki, T. Sato, V. Soloshonok, Asymmetric synthesis of α-amino acids via homologation of Ni(II) complexes of glycine Schiff bases. Part 2: Aldol, Mannich addition reactions, deracemization and (S) to (R) interconversion of α-amino acids, *Amino Acids* 45 (2013) 1017–1033;
 (b) A.E. Sorochinsky, J.L. Aceña, H. Moriwaki, T. Sato, V.A. Soloshonok, Asymmetric synthesis of α-amino acids via homologation of Ni(II) complexes of glycine Schiff bases; Part 1: alkyl halide alkylations, *Amino Acids* 45 (2013) 691–718.
- [9] T.A. Stephenson, G. Wilkinson, New complexes of ruthenium(II) and (III) with triphenylphosphine, triphenylarsine, trichlorostannate, pyridine and other ligands, *J. Inorg. Nucl. Chem.* 28 (1966) 945–956.
- [10] P.A. Anderson, G.B. Deacon, K.H. Haarmann, F.R. Keene, T.J. Meyer, D.A. Reitsma, B.W. Skelton, G.F. Strouse, N.C. Thomas, J.A. Treadway, A.H. White, Designed synthesis of mononuclear tris(heteroleptic) ruthenium complexes containing bidentate polypyridyl ligands, *Inorg. Chem.* 34 (1995) 6145–6157.
- [11] M.A. Bennett, T.N. Huang, T.W. Matheson, A.K. Smith, Di-μ-chloro-bis [chloro(η⁵-1-isopropyl-4- methyl-benzene)ruthenium(II)], *Inorg. Synth.* 21 (1982) 75.
- [12] A.A. Batista, C. Pereira, S.L. Queiroz, L.A.A. Oliveira, R.H.A. Santos, M.T.P. Gambardella, Nitrosyl ruthenium complexes with general formula [RuCl₃(NO)(P-P)] (P-P = [PPh₂(CH₂)nPPh₂], n = 1–3 and {PPh₂-CH=CH-PPh₂}). X-ray structure of [RuCl₃(NO)[PPh₂(CH₂)₃PPh₂]}, *Polyhedron* 16 (1997) 927–931.
- [13] E. Alessio, G. Mestroni, G. Nardin, W.M. Attia, M. Calligaris, G. Sava, S. Zorzet, *Cis*- and *trans*-dihalotetrakis(dimethyl sulfoxide)ruthenium(II) complexes (RuX₂(DMSO)₄; X = Cl, Br): synthesis, structure, and antitumor activity, *Inorg. Chem.* 27 (1988) 4099–4106.
- [14] M.O. Albers, T.V. Ashworth, H.E. Oosthuizen, E. Singleton, (η⁴-1,5-cyclooctadiene)ruthenium(II) complexes, *Inorg. Synth.* 26 (1989) 68–69.
- [15] G.M. Sheldrick, SADABS, University of Göttingen, Germany, 1996.
- [16] (a) G.M. Sheldrick, SHELXTL Software Reference Manual, Bruker AXS Inc., Madison, WI, 1997, Version 5.1.;
 (b) G.M. Sheldrick, A short history of SHELXTL, *Acta Crystallogr. Sect. A* 64 (2008) 112–122.
- [17] M. Sieger, B. Sarkar, S. Záliš, J. Fiedler, N. Escola, F. Doctorovich, J.A. Olabec, W. Kain, Establishing the NO oxidation state in complexes [Cl₅(NO)M]ⁿ⁺, M = Ru or Ir, through experiments and DFT calculations, *Dalton Trans.* (2004) 1797–1800.
- [18] B.L. Haymore, J.A. Ibers, Comparison of linear nitrosyl and singly bent aryl diazo complexes of ruthenium. Structures of trichloronitrosylbis(triphenylphosphine)ruthenium, RuCl₃(NO)(P(C₆H₅)₃)₂, and trichloro(p-tolyl)diazobis(triphenylphosphine)ruthenium-dichloromethane, RuCl₃(p-NC₆H₄CH₃)-(P(C₆H₅)₃)₂·CH₂Cl₂, *Inorg. Chem.* 14 (1975) 3060–3070.
- [19] L.-M. Shi, X.-X. Wang, X.-F. Ma, A.-Q. Jia, Q.-F. Zhang, Ruthenium(III)-carbonyl and ruthenium(II)-nitrosyl complexes of nitrogen-containing ligands with ethoxysilane groups, *J. Coord. Chem.* 69 (2016) 2630–2636.
- [20] F. Roncaroli, M. Videla, L.D. Slep, J.A. Olabe, New-features in the redox coordination chemistry of metal nitrosyls [M-NO⁺; M-NO; M-NO-(HNO)], *Coord. Chem. Rev.* 251 (2007) 1903–1930.
- [21] X.-F. Yin, H. Lin, A.-Q. Jia, Q. Chen, Q.-F. Zhang, Synthesis, structural characterization, and catalytic activity of ruthenium(II) monocarbonyl complexes with bidentate Schiff base and triphenylphosphine ligands, *J. Coord. Chem.* 66 (2013) 3229–3240.
- [22] Y.-F. Xie, H. Zhu, H.-T. Shi, A.-Q. Jia, Q.-F. Zhang, Ruthenium complexes containing pyridine-2,6- dicarboxylato ligands, *Inorg. Chim. Acta* 428 (2015) 147–153.
- [23] (a) R. Abbel, K. Abdur-Rashid, M. Faatz, A. Hadzovic, A.J. Lough, R.H. Morris, A succession of isomers of ruthenium dihydride complexes. Which one is the ketone hydrogenation catalyst? *J. Am. Chem. Soc.* 127 (2005) 1870–1882;
 (b) A.A. Rachford, J.L. Petersen, J.J. Rack, Designing molecular bistability in ruthenium dimethyl sulfoxide complexes, *Inorg. Chem.* 44 (2005) 8065–8075;
 (c) M. Jimenez-Tenorio, M.C. Puerta, P. Valerga, Atom-economical synthesis of the versatile ruthenium precursor [TpRuCl(COD)] (Tp = hydrotris(pyrazol-1-yl) borate) discloses a diamine ligand dealylation process, *Organometallics* 34 (2015) 1001–1004.
- [24] Ö. Aksin, H. Türkmen, L. Artok, B. Çetinkaya, C. Ni, O. Büyükgüngör, E. Özkal, Effect of immobilization on catalytic characteristics of saturated Pd-N-heterocyclic carbenes in Mizoroki–Heck reactions, *J. Organomet. Chem.* 691 (2006) 3027–3036.
- [25] S. Syukri, A. Sakthivel, W. Sun, F.E. Kühn, Immobilization of Ru(II)(salen)(PPh₃)₂ on mesoporous MCM-41/SBA-15: characterization and catalytic applications, *Catal. Lett.* 128 (2009) 18–24.
- [26] N. Linares, A.E. Sepúlveda, M.C. Pacheco, J.R. Berenguer, E. Lalinde, C. Nájera, J. García-Martínez, Synthesis of mesoporous metal complex-silica materials and their use as solvent-free catalysts, *New J. Chem.* 35 (2011) 225–234.
- [27] R.Q. Meng, B. Wang, H.-M. Sui, B. Li, W. Song, L.-X. Wu, B. Zhao, L.-H. Bi, Organoruthenium-supported polyoxotungstate – synthesis, structure and oxidation of n-hexadecane with air, *Eur. J. Inorg. Chem.* 10–11 (2013) 1935–1942.
- [28] E.K. Huang, W.-M. Cheung, K.-W. Chan, F.L.-Y. Lam, X. Hu, Q.-F. Zhang, I.D. Williams, W.-H. Leung, Alkylruthenium complexes containing polypyridyl ligands: synthesis, characterization, and immobilization on silica, *Eur. J. Inorg. Chem.* (2013) 2893–2899.

- [29] M.G. Bhowon, H.L.K. Wah, W.R. Narain, Schiff base complexes of ruthenium(II) and their use as catalytic oxidants, *Polyhedron* 18 (1999) 341–345.
- [30] (a) A. Choualeb, J. Rose, P. Braunstein, R. Welter, Routes to ruthenium-cobalt clusters and dicobalt complexes with new alkoxy-silyl- or sulfur-functionalized alkynes. X-ray structures of $[\text{NEt}_4][\text{RuCo}_3(\text{CO})_{10}(\mu_4\text{-}\eta^2\text{-HC}_2(\text{CH}_2)_2\text{OC(O)-NH(CH}_2)_3\text{Si(OEt)}_3)]$ and $[\text{Co}_2(\text{CO})_6(\mu_2\text{-}\eta^2\text{-HC}_2\text{CH}_2\text{NHC(O)-NH(CH}_2)_3\text{Si(OEt)}_3)]$, *Organometallics* 22 (2003) 2688–2693;
- (b) G. Gervasio, D. Marabello, E. Sappa, A. Secco, Reactions of $\text{Ru}_3(\text{CO})_{12}$ with ene-yne and alkoxy-silyl functionalized compounds. The crystal structure of $(\mu\text{-H})\text{Ru}_3(\text{CO})_9(\mu_3\text{-}\eta^2\text{-HC=N(CH}_2)_3\text{Si(OEt)}_3)$, *J. Cluster Sci.* 18 (2007) 67–85;
- (c) M. Knorr, P. Braunstein, A. Messaoudi, A. Tiripicchio, F. Uguzzoli, Synthesis and crystal structure of a heteronuclear Fe–Ru silyl complex, *J. Cluster Sci.* 18 (2007) 289–301;
- (d) F. Carniato, G. Gatti, G. Gervasio, D. Marabello, E. Sappa, A. Secco, Synthesis and structure of new phosphine-substituted homo- and hetero-bimetallic carbonyl clusters of iron, ruthenium and nickel. Characterization of two inorganic–organometallic hybrid materials based on mesoporous SBA-15 silica, *Inorg. Chim. Acta* 363 (2010) 1773–1778;
- (e) I. Karame, M. Boualleg, J.-M. Camus, T.K. Maishal, J. Alauzun, J.-M. Basset, C. Coperet, R.J.P. Corriu, R. Jeanneau, A. Mehdi, C. Reye, L. Veyre, C. Thieuleux, Tailored Ru-NHC heterogeneous catalysts for alkene metathesis, *Chem. Eur. J.* 15 (2009) 11820–11823.